

Identification of a Critical Residue in the Transmembrane Domain 2 of Tachykinin Neurokinin 3 Receptor Affecting the Dissociation Kinetics and Antagonism Mode of Osanetant (SR 142801) and Piperidine-Based Structures

Pari Malherbe,^{*,†} Claudia Kratzeisen,[†] Anne Marcuz,[†] Marie-Thérèse Zenner,[†] Matthias H. Nettekoven,[‡] Hasane Ratni,[‡] Joseph G. Wettstein,[†] and Caterina Bissantzi[‡]

[†]Discovery Research CNS and [‡]Chemistry, F. Hoffmann-La Roche Ltd., PRDN, Building 69/333, CH-4070 Basel, Switzerland

Received June 29, 2009

In this study, we show that compound **3** (osanetant) binds with a pseudoirreversible, apparent noncompetitive mode of antagonism at the guinea pig NK₃, while it behaves competitively at the human NK₃. This difference is caused by a slower dissociation rate of compound **3** at the guinea pig NK₃ compared to human NK₃. The only amino acid difference between the human and guinea pig NK₃ in the binding site (Thr139^{2,58} in human, corresponding to Ala114^{2,58} in guinea pig) has been shown to be responsible for the different behavior. Compound **1** (talnetant), however, behaves competitively at both receptors. Using these data, 3D homology modeling, and site-directed mutagenesis, a model has been developed to predict the mode of antagonism of NK₃ antagonists based on their binding mode. This model was successfully used to predict the mode of antagonism of compounds of another chemical series including piperidine-based structures at human and guinea pig NK₃.

Introduction

The neurokinins (NKs, also called tachykinins⁴) belong to a family of neuropeptides that mainly comprises the substance P (SP), neurokinin A (NKA), and neurokinin B (NKB). They elicit their effect through three G-protein-coupled receptors (GPCRs) called NK₁, NK₂, and NK₃ (nomenclature follows Alexander et al., 2008¹) that are coupled via G_{q/11} to the activation of phospholipase C, leading to an elevation of intracellular Ca²⁺ levels. The tachykinins rank order of potency at the NK receptors: SP > NKA > NKB for the NK₁, NKA > NKB > SP for the NK₂, and NKB > NKA > SP for the NK₃.^{2,3} The comparative studies using [³H]senktide autoradiography revealed striking differences in the CNS localization of NK₃ among rat, gerbil, and guinea pig⁴ and between some of these species and primates.⁵ In general, the expression of NK₃ (by in situ hybridization histochemistry and NKB/senkide binding) was detected in brain regions that include cortex (frontal, parietal, and cingulate cortex), various nuclei of the amygdala, the hippocampus, and midbrain structures (the substantia nigra, ventral tegmental area, and raphe nuclei).^{4,6,7} The distribution of NK₃ has been reported in the prefrontal and visual cortex of the human brain by immunohistochemistry.⁸

The tachykinins are involved in numerous physiological functions including nociception, neuroimmunomodulation, and reproduction. NK receptor dysfunction has been implicated in the pathology of various diseases such as emesis,

bronchial asthma, gastrointestinal disorders, inflammatory bowel syndrome, urinary bladder, and psychiatric disorders.^{9–11} Preclinical studies have demonstrated the involvement of NK₃-mediated activation in the release of dopamine, especially in ventral and dorsal striatal region.^{12,13} (S)-(+)-N-((3-[1-Benzoyl-3-(3,4-dichlorophenyl)piperidin-3-yl]propyl)-4-phenylpiperidin-4-yl)-N-methylacetamide (osanetant, SR 142801)^{14,15} and (S)-(-)-N-(α-ethylbenzyl)-3-hydroxy-2-phenylquinoline-4-carboxamide (talnetant, SB 223412),^{16,17} which are from two distinct chemical classes, have been shown to be potent nonpeptide antagonists of the NK₃. Both antagonists have been studied in schizophrenia patients in a double blind placebo controlled (short-term) clinical trial that suggested significant improvement in psychopathology, including positive symptoms.¹⁸ The information about phase II clinical trial of **3** (osanetant) showed the compound to be active in schizophrenia patients with improved efficacy, side effect profiles, and good tolerability.¹⁹ Recent clinical investigation of **1** (talnetant) in healthy volunteers has shown that it had psychomotor and cognitive effects and was able to improve visuomotor coordination and vigilance.²⁰

Although compound **1** clearly displayed a reversible and competitive mode of antagonism in the NKB-induced Ca²⁺ mobilization at cloned human NK₃ and in the senktide-induced contractions in rabbit isolated iris sphincter muscles,^{16,17} there have been controversial data regarding the inhibition mode of compound **3**. Investigations using [MePhe⁷]NKB- and senktide-stimulated inositol phosphate (IP) formation at the cloned human NK₃ or [MePhe⁷]NKB-mediated contractions of guinea pig ileum have shown a competitive mode of antagonism by compound **3**.^{14,21} However, many other studies that used senktide- and [MePhe⁷]NKB-mediated contractions of the guinea pig isolated ileum longitudinal muscle preparation or senktide-induced

*To whom correspondence should be addressed. Phone: +41-61-688-6286. Fax: +41-61-688-1720. E-mail: parichehr.malherbe@roche.com.

^aAbbreviations: NK, neurokinin; NK₃, neurokinin 3 receptor; GPCRs, G-protein coupled receptors; NKB, neurokinin B; IP, inositol phosphates; 7TMD, seven-transmembrane domain; WT, wild-type; OPSD, bovine rhodopsin.

Table 1. Schild Constants for Antagonism of [MePhe⁷]NKB-Induced Accumulation of [³H]IP by NK₃ Antagonists in the HEK293 Cells Transiently Expressing hNK₃-WT, gpNK₃-WT, or gpNK₃-A114^{2.58T}^a

NK ₃ antagonist	hNK ₃ -WT			gpNK ₃ -WT			gpNK ₃ -A114 ^{2.58T}		
	pA ₂	Schild slope	mode of antagonism	pA ₂	Schild slope	mode of antagonism	pA ₂	Schild slope	mode of antagonism
1	8.24	0.88	competitive	7.81	1.07	competitive	7.91	1.12	competitive
3	7.73	1.59	competitive			noncompetitive	8.5	1.03	competitive
5	8.05	0.99	competitive			noncompetitive	7.96	1.32	competitive
6	8.11	0.85	competitive			noncompetitive	7.83	0.76	competitive
7	7.74	1.24	competitive	7.62	1.25	competitive	7.53	0.97	competitive

^aThe apparent antagonist potency (pA₂) and Schild slope values were determined from Schild plot analyses.

formation of [³H]IP in slices from the guinea pig ileum all pointed to a noncompetitive, insurmountable, and long-lasting irreversible antagonism by compound **3**.^{15,22,23} A recent study, which compared antagonism modes of compounds **1** and **3** in cellular Ca²⁺ mobilization and binding kinetics, has demonstrated that both antagonists displayed a competitive mode of antagonism at recombinant human NK₃.²⁴ Furthermore, site-directed mutagenesis and molecular modeling studies have indicated that (*S*)-(-)-*N*-(α -ethylbenzyl)-3-methoxy-2-phenylquinoline-4-carboxamide (Me-talnetant) and compound **3** interact within overlapping but not identical binding pockets in the human NK₃ 7TMD.²⁵ Taken together, these studies are consistent with the notion that the guinea pig NK₃ receptor has to be responsible for the compound **3**'s apparent noncompetitive (pseudoirreversible) mode of antagonism.

In the current study, we have compared the compound **3**'s mode of antagonism at human and guinea pig NK₃ wild-type and mutated receptors by binding kinetics and functional Schild analysis using [MePhe⁷]NKB-induced formation of [³H]IP assay. This data, together with rhodopsin-based 3D modeling and site-directed mutagenesis, allowed development of a model that predicts the mode of antagonism of NK₃ antagonists based on their predicted docking poses. We have validated this model by testing its capability to predict the antagonism mode of three piperidine derivatives, 2-(3,4-dichlorophenyl)-*N*-(4-fluoro-3-trifluoromethylbenzyl)-2-*N*-dimethyl-4-[4-(2-oxo-pyrrolidin-1-yl)-piperidin-1-yl]-butyramide (**5**), 4-[4-(acetylmethyl-amino)-piperidin-1-yl]-2-(3,4-dichlorophenyl)-*N*-(4-fluoro-3-trifluoromethylbenzyl)-2-*N*-dimethylbutyramide (**6**), and 4-[4-(acetylmethyl-amino)-piperidin-1-yl]-*N*-(2-chloro-benzyl)-2-(3,4-dichlorophenyl)-2-*N*-dimethylbutyramide (**7**)²⁶ at the human NK₃ and guinea pig NK₃-WT and mutated receptors.

Results

Comparison of the Mode of Antagonism of Compounds 1 and 3 at Human and Guinea Pig NK₃ Receptors. To compare the inhibition mode of NK₃ antagonists at hNK₃ and gpNK₃, the concentration–response curves (CRCs) for [³H]IP formation stimulated by [MePhe⁷]NKB were measured in the absence or presence of increasing concentrations of antagonist in the HEK cells transiently transfected with hNK₃ or gpNK₃. [MePhe⁷]NKB was used as agonist because it has a high selectivity for hNK₃ (*K*_i value of 0.3 nM) versus hNK₂ (*K*_i value of 1597 nM).¹⁷ [MePhe⁷]NKB elicited concentration-dependent increases in the accumulation of [³H]IP in the hNK₃ expressing cells with the EC₅₀ and *n*_H values of 0.6 ± 0.0 nM and 1.0 ± 0.0, respectively, and in the gpNK₃ expressing cells with the EC₅₀ and *n*_H values of 0.6 ± 0.0 nM and 1.0 ± 0.1, respectively. The apparent antagonist potency (pA₂) and the Schild slope values calculated from

[MePhe⁷]NKB Schild analyses are given in Table 1. Compound **1** behaved as a competitive antagonist at both hNK₃ and gpNK₃, shifting the NKB CRCs to the right without changing its maximal response (Figure 1A,B and Table 1). Compound **3** behaved in a competitive manner at hNK₃ (Figure 2A and Table 1), but it displayed a noncompetitive like mode of antagonism at gpNK₃ (Figure 2B).

The alignment of the amino acids forming the NK₃ binding pocket among various species is shown in Figure 3. The only amino acid difference between human and guinea pig is the residue Thr139^{2.58} in human NK₃, which corresponds to Ala114^{2.58} in guinea pig NK₃ (Figure 3). Hence, guinea pig NK₃-Ala114^{2.58} was converted to Thr114^{2.58}. Because the mutation gpNK₃-A114^{2.58T} had no effect on [MePhe⁷]NKB potency (EC₅₀ and *n*_H values of 0.9 ± 0.1 nM and 1.1 ± 0.1, respectively), the antagonism mode of compounds **1** and **3** was compared at the mutated gpNK₃-A114^{2.58T} receptor using Schild analyses. While the mutation of gpNK₃-A114^{2.58T} had no effect on competitive mode of antagonism by compound **1** (Figure 1C,D and Table 1), it yet converted compound **3**'s noncompetitive mode of antagonism to a competitive one (Figure 2C, D and Table 1).

Binding Affinity of NK₃ Antagonists at Various NK Receptors as Measured by Displacement Studies. The affinity constants of NK₃ antagonist in the membrane preparations from HEK293 cells transiently expressing hNK₁, hNK₂, hNK₃, gpNK₃, or gpNK₃-A114^{2.58T} are given in Table 2. Both compounds **1** and **3** bind with similar affinity to hNK₃, gpNK₃, and gpNK₃-A114^{2.58T} (Table 2). Compounds **5**, **6**, and **7** (piperidine derivatives) are potent and selective hNK₃ antagonists (Table 2), and their structures are shown in Figure 4.²⁶ As seen in Table 2, all three compounds also displayed similar affinity for hNK₃, gpNK₃, and gpNK₃-A114^{2.58T}. Therefore, the mutation gpNK₃-A114^{2.58T} had no effect on binding affinities of NK₃ antagonists.

Comparison of Binding Kinetics of Radioligand [³H]3 ([³H]SR 142801) to hNK₃-WT, gpNK₃-WT, and gpNK₃-A114^{2.58T}. Binding kinetics of radioligand [³H]3 to membrane preparations from HEK293 cells transiently expressing hNK₃-WT, gpNK₃-WT, and gpNK₃-A114^{2.58T} are shown in Figure 5 and the kinetic parameters in Table 3. Binding of radioligand [³H]3 to the hNK₃-WT was rapid with half-maximal binding occurring at 4 min and reaching equilibrium within 30 min (Figure 5A and Table 3). The association bindings of radioligand [³H]3 to the gpNK₃-WT and gpNK₃-A114^{2.58T} were similar with half-maximal binding, *t*_{1/2} values of 10.2 and 10.0 min, respectively (Figure 5A and Table 3). The data for three receptors were fit to a one-phase exponential model (Figure 5A).

The dissociation rates for radioligand [³H]3 bindings to the hNK₃-WT, gpNK₃-WT, and gpNK₃-A114^{2.58T} were determined by the addition of an excess amount of (*S*)-(-)-*N*-(α -ethylbenzyl)-3-methyl-2-phenylquinoline-4-carboxamide (SB

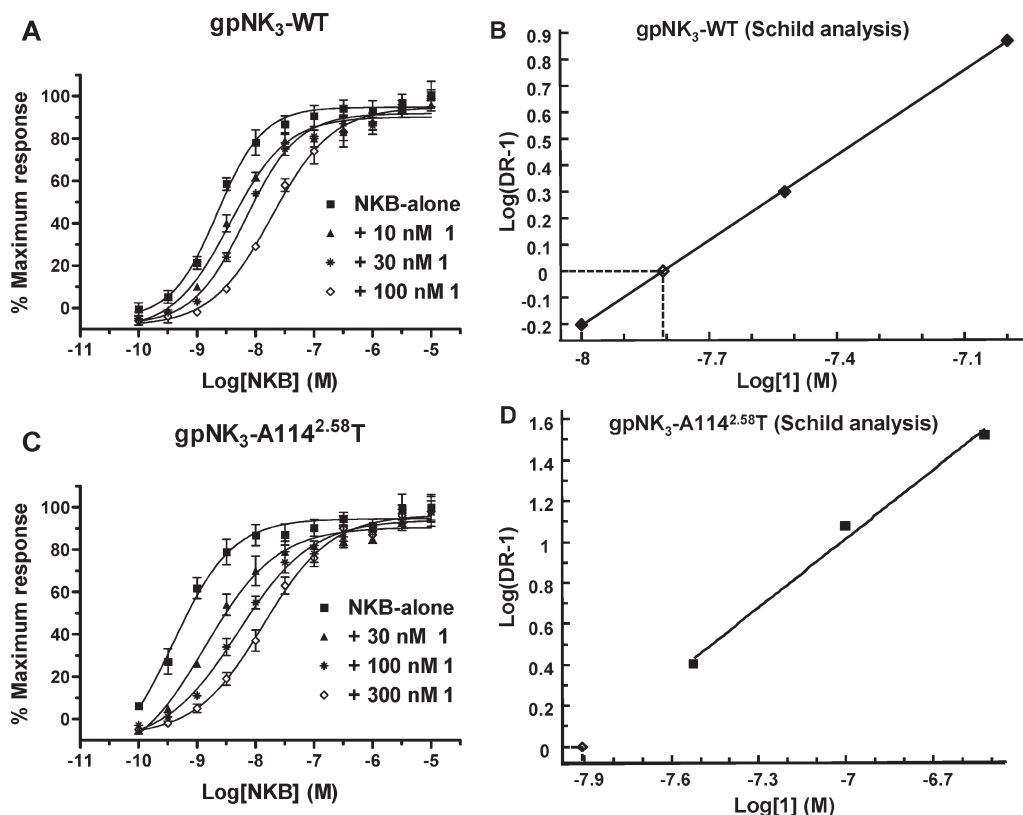


Figure 1. Schild plot analyses for antagonism of [MePhe⁷]NKB-induced accumulation of [³H]IP by compound **1** (talnetant). Concentration–response curves (CRCs) for [³H]IP formation stimulated by [MePhe⁷]NKB in the absence and presence of various concentrations of compound **1** in HEK293 cells expressing transiently the gpNK₃-WT (A) and gpNK₃-A114^{2.58T} (C). Schild plots for antagonism by compound **1** at gpNK₃-WT (B) and gpNK₃-A114^{2.58T} (D). The EC₅₀ and EC₅₀' values, which derived from NKB CRCs in the absence and presence of increasing fixed concentrations of compound **1** (A,C) were used to calculate the dose ratios (DR = EC₅₀'/EC₅₀) and plotted according to Schild regression in (B) and (D). Each curve represents the mean of six concentration–response measurements from three independent transfections.

222200)¹⁶ after equilibrium was reached. The reversals of bindings from hNK₃-WT and gpNK₃-A114^{2.58T} were complete, with *t*_{1/2} values of 10 and 17 min, respectively (Figure 5B and Table 3). The rate of radioligand [³H]**3** dissociation from the gpNK₃ was decreased as compared to the hNK₃-WT (Figure 5B and Table 3). The calculations of the apparent *K*_d values derived from the kinetic experiments are given in Table 3. The radioligand [³H]**3** had an apparent *K*_d value of 0.22 ± 0.06 nM at WT receptor, which is in good agreement with the equilibrium *K*_d value (0.20 ± 0.01). However, the apparent *K*_d values of radioligand [³H]**3** at the gpNK₃ (0.08 ± 0.01 nM) was lower than that of equilibrium *K*_d values (0.15 ± 0.03). Conversely, it had a higher apparent *K*_d value (0.12 ± 0.03 nM) than that of equilibrium *K*_d value (0.08 ± 0.01 nM) at gpNK₃-A114^{2.58T}.

Inhibition Mode of Compounds 5, 6, and 7 on the [MePhe⁷]NKB-Evoked Accumulation of [³H]IP at hNK₃, gpNK₃, and gpNK₃-A114^{2.58T}. To explore the chemical moiety that is involved in NK₃ antagonists' mode of action, three piperidine derivatives, compounds **5**, **6**, and **7**, were further investigated in the NKB-induced formation of [³H]IP assay in HEK293 cells expressing transiently the hNK₃, gpNK₃ and gpNK₃-A114^{2.58T}. The choice of these antagonists was guided by our docking model that predicted compounds **5** and **6** to have a noncompetitive mode of antagonism and compound **7** a competitive one. All three NK₃ antagonists behaved competitively at hNK₃ (Table 1). As predicted, both compounds **5** and **6** acted in a noncompetitive manner at gpNK₃ and a competitive one when the

mutated guinea pig receptor was used (Figure 6A–D and Table 1), while compound **7** displayed a competitive mode of antagonism at both gpNK₃ and gpNK₃-A114^{2.58T} (Figure 6E,F and Table 1).

Discussion and Conclusion

Phase II clinical results of compounds **1** and **3** have indicated that blocking the NK₃ receptor could be beneficial for the treatment of schizophrenia and possibly other psychoses.^{18,19} Therefore, NK₃ antagonists represent an alternative therapeutical approach for the treatment of schizophrenia.²⁷ Species-related differences in the pharmacology of NK₃ antagonists have been reported, especially between human and mouse/rat NK₃. Thus, two residues in TM2, Met134^{2.53} and Ala146^{2.65} of hNK₃, which correspond to Val121^{2.53} and Gly133^{2.65} of mouse, are shown to be involved in the species-selectivity of *N*-[(*S*)-4-(4-acetylamino-4-phenyl-piperidin-1-yl)-2-(3,4-dichloro-phenyl)-butyl]-*N*-methyl-benzamide (SR 48968, **4**) (a close derivative of compound **3**) for hNK₃.^{28,29} However, there is no such report concerning guinea pig and selective NK₃ antagonists. As compounds **1** and **3** have displayed similar potency at human and guinea pig NK₃ receptors, human-like pharmacology of guinea pig NK₃ has made an appropriate species for characterization of the in vivo efficacy of NK₃ antagonists.³⁰ In the current study, we have attempted to resolve the controversy about compound **3**'s antagonism mode of action between human and guinea pig receptors.

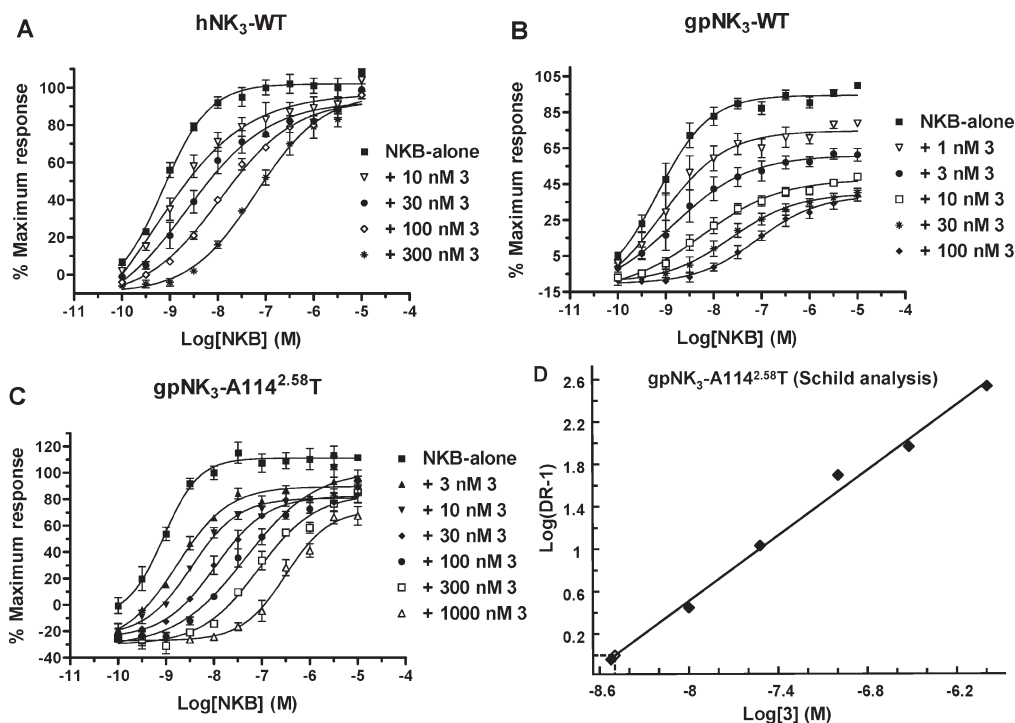


Figure 2. Schild analyses showing the competitive like mode of antagonism by compound **3** (osanetant) at hNK₃-WT and gpNK₃-A114^{2.58T} and noncompetitive one at gpNK₃-WT. CRCs for [³H]IP formation stimulated by [MePhe⁷]NKB in the absence or presence of increasing concentrations of compound **3** in HEK293 cells expressing transiently the hNK₃-WT (A), gpNK₃-WT (B), and gpNK₃-A114^{2.58T} (C). Schild plot for antagonism by compound **3** at gpNK₃-A114^{2.58T} is shown in (D). Each curve represents the mean of six concentration–response measurements from three independent transfections.

GPCR	1.35	1.39	1.42	1.46	2.53	2.57	2.58	2.61	2.65	3.28	3.29	3.32	3.33	3.35	3.36	3.37	3.40	4.60	45.49	5.38	5.39	5.42	5.43	5.46	5.47	6.44	6.48	6.51	6.52	6.55	7.35	7.38	7.39	7.40	7.42	7.43	7.45
NK3R_RAT	W	Y	V	A	V	N	T	N	G	Q	N	P	I	A	V	F	I	Q	L	Y	H	V	I	V	Y	F	W	Y	H	F	Y	S	F	W	A	M	S
NK3R_MOUSE	W	Y	V	A	V	N	T	N	G	Q	N	P	I	A	V	F	I	Q	L	Y	H	V	I	V	Y	F	W	Y	H	F	Y	S	F	W	A	M	S
NK3R_GERBIL	W	Y	V	A	M	N	T	N	A	Q	N	P	I	A	V	F	I	Q	L	Y	H	V	I	V	Y	F	W	Y	H	F	Y	S	F	W	A	M	S
NK3R_HUMAN	W	Y	V	A	M	N	T	N	A	Q	N	P	I	A	V	F	I	Q	L	Y	H	V	I	V	Y	F	W	Y	H	F	Y	S	F	W	A	M	S
NK3R_CAVPO	W	Y	V	A	M	N	A	N	A	Q	N	P	I	A	V	F	I	Q	L	Y	H	V	I	V	Y	F	W	Y	H	F	Y	S	F	W	A	M	S
NK3R_CANINE	W	Y	V	A	M	N	T	N	A	Q	N	P	I	A	V	F	I	Q	L	Y	H	V	I	V	Y	F	W	Y	H	F	Y	S	F	W	A	M	S
NK3R_CYNOMOLGUS	W	Y	V	A	M	N	T	N	A	Q	N	P	I	A	V	F	I	Q	L	Y	H	V	I	V	Y	F	W	Y	H	F	Y	S	F	W	A	M	S
NK1R_HUMAN	W	Y	I	S	M	N	T	N	A	H	N	P	I	A	V	F	I	Q	V	Y	H	V	T	I	Y	F	W	F	H	F	Y	I	M	W	A	M	S
NK2R_HUMAN	W	Y	L	A	M	N	A	N	A	Q	N	P	I	A	M	F	I	Q	K	Y	H	V	I	I	Y	F	W	Y	H	F	Y	L	F	W	A	M	S
OPSD_BOVIN	L	M	L	G	M	G	F	T	S	E	G	A	T	G	G	E	L	P	S	F	V	M	F	H	F	F	W	Y	A	A	M	P	A	F	A	K	S

Figure 3. Alignment of the amino acids forming the binding site. The first row gives the Ballesteros–Weinstein numbering scheme. The numbers above the NK3R_HUMAN and NK3R_CAVPO receptors give the sequence number of the positions of the mutations carried out in this study. The amino acid sequences of the rat NK₃ (accession number: P16177), mouse NK₃ (accession number: P47937), gerbil NK₃ (accession number: AM157740), human NK₃ (accession number: P29371), guinea pig NK₃ (accession number: P30098), dog NK₃ (accession number: AM423140), cynomolgus monkey NK₃ (in-house data), human NK₁ (accession number: P25103), and human NK₂ (accession number: P21452) were retrieved from the Swiss-Prot database.

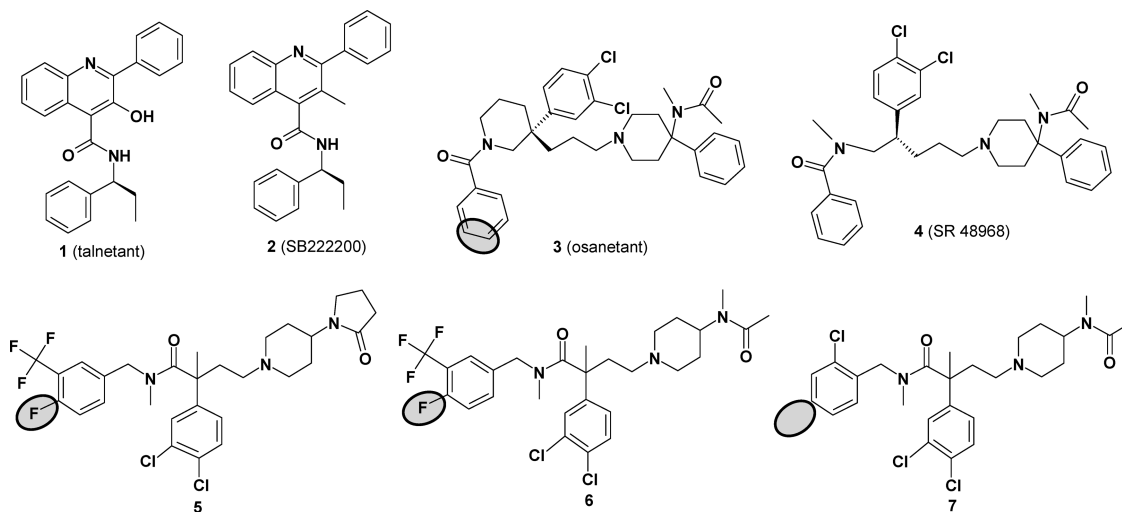
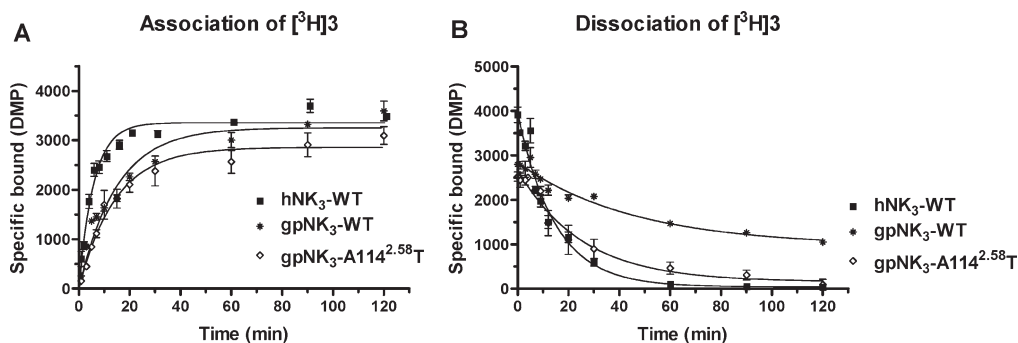
Investigation of the antagonistic mechanism of compounds **1** and **3** revealed that both compounds act as competitive antagonists at hNK₃. Compound **1** still had a competitive mode of antagonism at gpNK₃, yet compound **3** behaved in a noncompetitive manner at gpNK₃. This mode of action was characterized by a rightward shift of the [MePhe⁷]NKB concentration–response curves (increase in EC₅₀ values) in the presence of increasing compound **3** concentrations with a concomitant large decrease in the maximal effect (*E*_{max}). To better understand the mechanism of compound **3**'s apparent noncompetitive behavior at gpNK₃, binding kinetics of

radioligand [³H]**3** were compared between guinea pig and human receptors. As expected, radioligand [³H]**3** had a slower dissociation rate at guinea pig receptor (the reversal of binding was incomplete and did not reach the baseline even after 2 h) in comparison to human one. This could be a possible explanation for the apparent noncompetitive and pseudoirreversible mode of antagonism by compound **3** at gpNK₃ determined by Schild plot analyses. Because of compound **3**'s slow dissociation, a large portion of the gpNK₃ is not available for activation by NKB, consequently, the maximally achievable response of NKB drops dramatically

Table 2. Binding Affinity of NK₃ Antagonists in the Membrane Preparations from HEK293 Cells Transiently Expressing hNK₁, hNK₂, hNK₃, gpNK₃, or gpNK₃-A114^{2.58T}^a

NK ₃ antagonist	³ H]SP hNK ₁		³ H]4 hNK ₂		³ H]3					
					hNK ₃		gpNK ₃		gpNK ₃ -A114 ^{2.58T}	
	K _i nM	n _H	K _i nM	n _H	K _i nM	n _H	K _i nM	n _H	K _i nM	n _H
1	> 10000		> 10000		3.0 ± 0.4	0.9 ± 0.1	5.0 ± 1.5	1.0 ± 0.1	3.8 ± 0.2	1.0 ± 0.0
3	209.6 ± 24.6	0.9 ± 0.2	35.5 ± 1.1	1.0 ± 0.0	0.5 ± 0.0	1.0 ± 0.0	0.6 ± 0.2	1.0 ± 0.1	0.8 ± 0.0	1.5 ± 0.0
5	181.6 ± 20.8	0.9 ± 0.0	108.6 ± 10.1	0.9 ± 0.0	0.8 ± 0.2	0.9 ± 0.1	1.6 ± 0.3	1.7 ± 0.5	1.8 ± 0.2	1.5 ± 0.1
6	151.8 ± 15.1	0.9 ± 0.1	515.3 ± 24.9	0.9 ± 0.1	3.1 ± 0.4	1.1 ± 0.1	3.5 ± 0.3	1.2 ± 0.1	2.7 ± 0.2	1.4 ± 0.0
7	70.9 ± 21.6	0.8 ± 0.1	952.6 ± 156.8	0.7 ± 0.1	10.4 ± 5.0	1.1 ± 0.0	8.0 ± 3.5	1.0 ± 0.0	11.9 ± 2.8	1.2 ± 0.1

^aThe affinity constant (K_i) and Hill slope (n_H) values for radioligands [³H]SP, [³H]4 ([³H]SR 48968), and [³H]3 ([³H]SR 142801) binding inhibitions by various antagonists were calculated as described in the Experimental Section. Values are mean ± SE of the K_i calculated from three independent experiments, each performed in duplicate.

**Figure 4.** Chemical structures of NK antagonists. The moiety that controls the mode of antagonism is indicated by the filled circle.**Figure 5.** Time course for the association (A) and dissociation (B) of radioligand [³H]3 binding to the hNK₃-WT, gpNK₃-WT, and gpNK₃-A114^{2.58T} membranes. Each data point is mean ± SE (bars) of three individual experiments performed in quadruplet.**Table 3.** Kinetic Parameters for Association and Dissociation of Radioligand [³H]3 in the hNK₃-WT, gpNK₃-WT, and gpNK₃-A114^{2.58T} Membranes^a

NK ₃ receptor	association kinetic			dissociation kinetic			
	K _{ob} min ⁻¹	K _{on} nM ⁻¹ min ⁻¹	t _{1/2} min	K _{off} min ⁻¹	t _{1/2} min	apparent K _d nM	equilibrium K _d nM
human	0.17 ± 0.02	0.33 ± 0.04	4.01 ± 0.73	0.07 ± 0.01	10.10 ± 1.07	0.22 ± 0.06	0.20 ± 0.01
guinea pig	0.068 ± 0.01	0.32 ± 0.06	10.23 ± 0.20	0.022 ± 0.01	31.5 ± 4.10	0.08 ± 0.01	0.15 ± 0.03
gpNK ₃ -A114 ^{2.58T}	0.07 ± 0.01	0.32 ± 0.05	9.9 ± 1.2	0.04 ± 0.01	17.43 ± 0.5	0.12 ± 0.03	0.08 ± 0.01

^aThe K_{ob} (observed on rate), K_{off} (observed off rate), K_{on}, t_{1/2} (half-maximal binding), and K_d (apparent dissociation constant) values are mean ± SE, calculated from three independent experiments (each performed in quadruplet) as described in the Experimental Section.

in comparison to fast dissociating antagonist such as compound **1**.

When the sequences of the NK₃ 7TMD were compared among seven species, it showed that, with the exception of

gpNK₃, which carries an alanine at position 114 (helix position 2.58), all other species have threonine at this position. This is also the only amino acid difference found in the 7TMD region between guinea pig and human. Indeed, the mutation

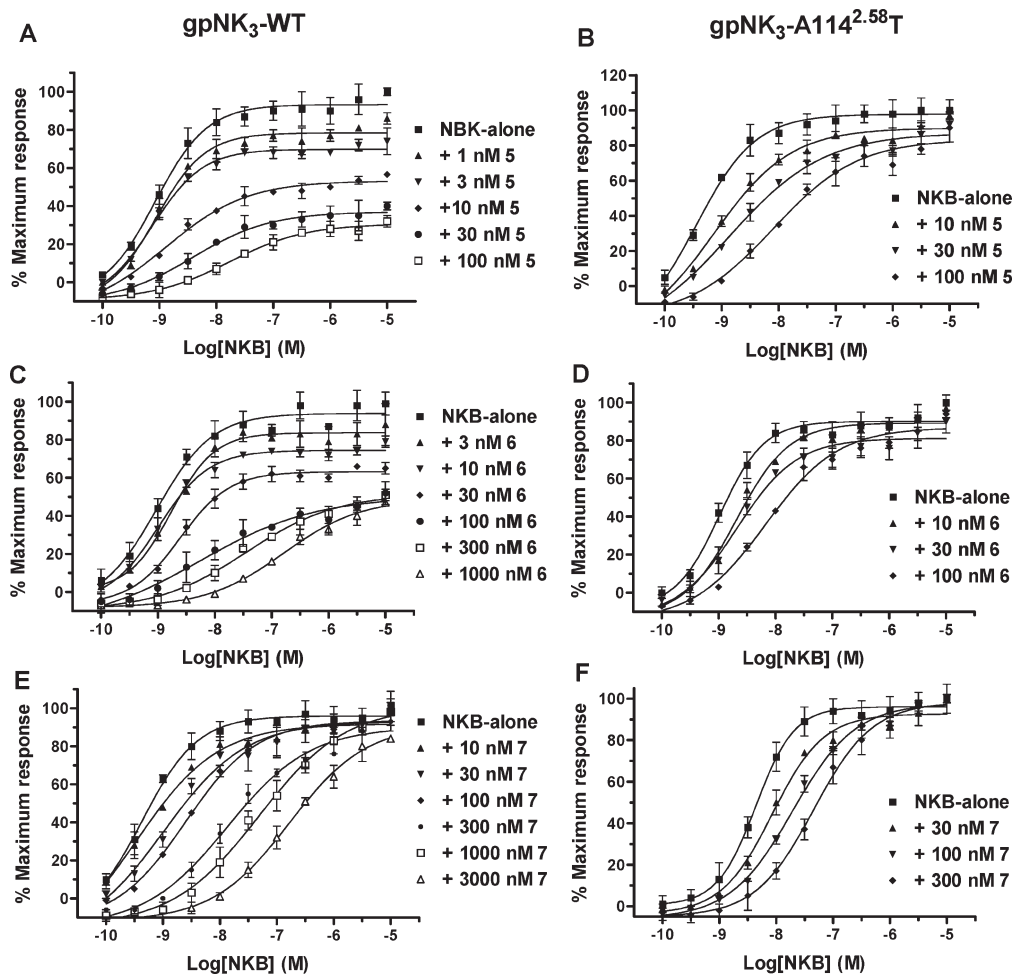


Figure 6. Schild plot analyses for antagonism of [MePhe⁷]NKB-induced accumulation of [³H]IP by compounds **5**, **6**, and **7**. Concentration–response curves for [³H]IP formation stimulated by [MePhe⁷]NKB in the absence and presence of various concentrations of compound **5** (A,B), compound **6** (C,D), and compound **7** (E,F) in HEK293 cells expressing transiently the gpNK₃-WT or gpNK₃-A114^{2.58}T. Each curve represents the mean of six concentration–response measurements from three independent transfections.

gpNK₃ A114^{2.58}T converted compound **3**'s apparent noncompetitive behavior to a competitive one and its slow dissociation to a fast one, very similar to human receptor. Interestingly, as we have shown previously, mutation of human NK₃ Thr139^{2.58} to alanine has conversely caused compound **3**'s competitive mode to be converted to a noncompetitive one while it had no effect on compound **1**'s competitive mode.²⁵ Therefore, Ala114^{2.58} was identified as the critical residue for the apparent noncompetitive mode of antagonism by compound **3** at the guinea pig versus its competitive one at human NK₃ Thr139^{2.58} receptor.

To visualize these data, we carefully analyzed the previously reported docking poses of compounds **1** and **3** onto the 7TMD binding cavity of the human NK₃ model (Figure 7A).²⁵ Strikingly, compound **3** locates two of its carbon atoms at a distance below 3 Å to the oxygen of hNK₃ Thr139^{2.58} (Figure 7B). At such a short distance (< 3 Å), the oxygen–aryl interaction is repulsive. On the other side, the distance to C β of gpNK₃ Ala114^{2.58} is within the favorable range of an alkyl–aryl interaction. Thus, compound **3** forms in gpNK₃, an additional attractive interaction that is not present in hNK₃. This change between an unfavorable situation in hNK₃ to a favorable one in gpNK₃ can explain the observed switch from fast to slow dissociation rate from hNK₃ to gpNK₃. On the other hand, compound **1**, which is not

affected by this mutation, does not locate any of its atoms close enough to residue 2.58 to generate a repulsive interaction with hNK₃ Thr139^{2.58} or a favorable one with gpNK₃ Ala114^{2.58}. Moreover, searches in the Cambridge Structural Database (www.ccdc.cam.ac.uk/products/csd/) validated our opinion that a distance below 3 Å is indeed repulsive for an oxygen–aryl interaction, the shortest observed distance for such interactions being 3.16 Å. Additionally, we analyzed the distance between alkyl–aryl groups. Here, the most favorable distance determined by a peak in the distance histogram is between 3.6 and 4.2 Å. It was thus concluded that the two carbon atoms of compound **3** located in the region close to 2.58 are responsible for the apparent noncompetitive behavior and slow dissociation rate of compound **3** at the guinea pig receptor. We then hypothesized that in general NK₃ antagonists with a heavy atom located in this region of the binding pocket should slow the dissociation rate at gpNK₃ and therefore show an apparent noncompetitive binding kinetics. Possible heavy atoms should be any that can form hydrophobic interactions with alanine and are repulsive to oxygen at a distance below 3 Å, therefore besides carbon, fluorine should also fulfill this criterion. Compounds of the piperidine series should hence be suitable to validate this hypothesis. In their predicted docking pose, derivatives with a para-substituted phenyl ring locate the para substituent onto compound

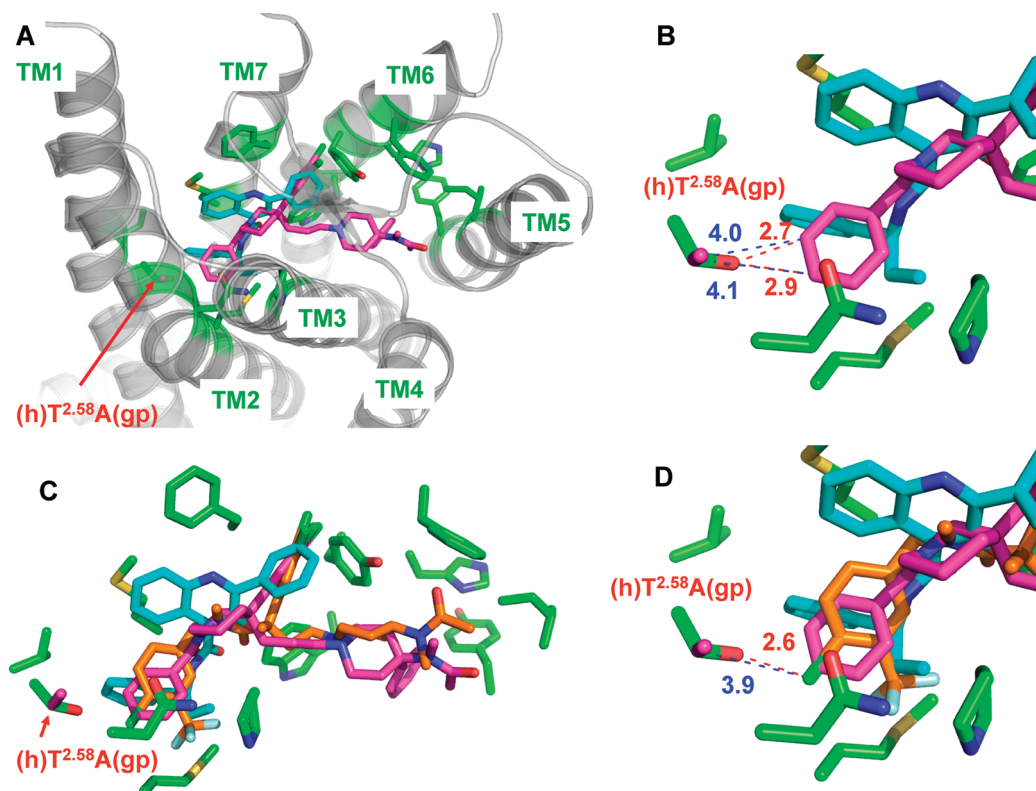


Figure 7. (A) Proposed docking poses of **3** (osanentan) (magenta) and **1** (talnetant) (blue) as described in our previous work.²⁵ (B) Zoom on the region of difference in the human and guinea pig receptor. The distances of the two carbon atoms of compound **3** that are closest to hNK₃ Thr139^{2.58} are displayed and given in Å: in red the distances to the oxygen atom of hNK₃ Thr139^{2.58}, in blue the distances to the C β of gpNK₃ Ala114^{2.58}. (C) Compound **6** (piperidine series, orange) docked additionally to compounds **1** (blue) and **3** (magenta) into the human NK₃. (D) Zoom on the region of difference between the two species with the same ligands as shown in (C). The distances of the fluorine atom of compound **6** to the residue in position 2.58 are displayed and given in Å: in red the distance to the oxygen atom of hNK₃ Thr139^{2.58}, in blue the distance to the C β of gpNK₃ Ala114^{2.58}.

3's carbon that is responsible for the apparent noncompetitive kinetics (Figure 7C,D). Thus, it was predicted that the para substituted derivatives, compounds **5** and **6**, should have an apparent noncompetitive behavior at gpNK₃ while para-H derivatives such as compound **7** should be competitive.

Compounds **5**, **6**, and **7** are potent and selective hNK₃ antagonists, their structures belonging to a chemical class different from compounds **1** and **3**. As predicted by modeling, compounds **5** and **6** showed an apparent noncompetitive mode of action, very much like compound **3**, at the gpNK₃, while compound **7** behaved competitively. The mutation A114^{2.58}T in gpNK₃ also converted the apparent noncompetitive behavior of compounds **5** and **6** to a competitive one, very similar to that of hNK₃-WT. This confirmed the hypothesis that the placement of a heavy atom close to Ala^{2.58} can trigger the apparent noncompetitive behavior at gpNK₃. Compounds **6** and **5**, differing in the piperidine substituent, showed that this part does not contribute to the special binding kinetics. Consequently, we have discovered a region in the binding site of the NK₃ receptor that is responsible for different modes of antagonism at hNK₃ and gpNK₃ when occupied by an antagonist carrying a hydrophobic atom like carbon or fluorine. In the hNK₃ receptor, antagonists with a heavy atom in this space show a fast dissociation rate; hence a competitive behavior because the interaction with hNK₃ Thr139^{2.58} is repulsive. In the gpNK₃, the interaction of a heavy atom in this region with gpNK₃ Ala114^{2.58} is attractive. By providing an anchor point, this additional favorable hydrophobic interaction is leading to a slower dissociation rate and thus an apparent noncompetitive behavior.

In conclusion, a single point mutation of guinea pig NK₃ receptor changes the mechanism of action of compound **3** by affecting its dissociation kinetics. To the best of our knowledge, this is the first time that binding kinetics is predictable across various chemical series on the rational basis of a common specific protein–ligand interaction. It remains to be shown whether similar key protein–ligand interactions can be found for the human NK₃ receptor. This would be of high importance because, as it has already been well documented in the case of angiotensin AT1 receptor and many other GPCRs,^{31–35} a noncompetitive (slow dissociating) antagonist should possess in vivo a much longer duration of action and greater efficacy than a competitive (rapidly dissociating) one.

Experimental Section

Chemistry. All reactions were carried out under argon atmosphere. Dry solvents and reagents of commercial quality were used as purchased. Column chromatography was carried out on silica gel 60 (32–60 mesh) or on prepacked columns (Isolute Flash Si). Proton NMR spectra were obtained on Bruker 300 or 400 MHz instrument with chemical shifts relative to tetramethylsilane as internal standard. Mass spectra were recorded on SSQ 7000 (Finnigan-MAT) for electron impact ionization. The purity of all final compounds was assessed by LC-MS and found above 99%.

(*S*)-(+)-*N*-((3-[1-Benzoyl-3-(3,4-dichlorophenyl)piperidin-3-yl]prop-1-yl)-4-phenylpiperidin-4-yl)-*N*-methylacetamide (**3**, osanentan, SR 142801),¹⁴ (*S*)-(-)-*N*-(α -ethylbenzyl)-3-methyl-2-phenylquinoline-4-carboxamide (**2**, SB 222200),¹⁶ (*S*)-(-)-*N*-(α -ethylbenzyl)-3-hydroxy-2-phenylquinoline-4-carboxamide (**1**, talnetant, SB

223412),¹⁶ (2*S*,3*S*)-*cis*-2-(diphenylmethyl)-*N*-[(2-methoxyphenyl)-methyl]-1-azabicyclo[2.2.2]octan-3-amine (CP-96,34),³⁶ and 1-{2-[(*R*)-3-(3,4-dichloro-phenyl)-1-(3,4,5-trimethoxy-benzoyl)-pyrrolidin-3-yl]-ethyl}-4-phenyl-piperidine-4-carboxylic acid amide (MDL 105,212)³⁷ were synthesized according to procedures described in published literature and their purity was confirmed (>99% by LC-MS analysis).

The preparation, NMR, and MS spectroscopic description of compounds 2-(3,4-dichlorophenyl)-*N*-(4-fluoro-3-trifluoromethyl-benzyl)-2,*N*-dimethyl-4-[4-(2-oxo-pyrrolidin-1-yl)-piperidin-1-yl]-butyramide (**5**),²⁶ 4-[4-(acetyl-methyl-amino)-piperidin-1-yl]-2-(3,4-dichloro-phenyl)-*N*-(4-fluoro-3-trifluoromethyl-benzyl)-2,*N*-dimethyl-butylamide (**6**),²⁶ and 4-[4-(acetyl-methyl-amino)-piperidin-1-yl]-*N*-(2-chloro-benzyl)-2-(3,4-dichloro-phenyl)-2,*N*-dimethyl-butylamide (**7**)²⁶ are described in the Supporting Information.

Materials. Radioligands [³H]**3** ([³H]SR 142801, catalogue no. TRK1035, specific activity: 74.0 Ci/mmol, radiochemical purity of 99.7% by HPLC, Novapak C18 column), [³H]SP ([³H]Substance P, catalogue no. TRK786, specific activity: 40.0 Ci/mmol), and [³H]**4** ([³H]SR 48968, catalogue no. TRK398, specific activity: 27.0 Ci/mmol, radiochemical purity of 97.8% by HPLC Aquapore RP-300 octyl 7 μm) were purchased from GE Healthcare UK limited, Chalfont St. Giles, UK. [MePhe⁷]Neurokinin B (Asp-Met-His-Asp-Phe-Phe-NMe-Phe-Gly-Leu-Met-NH₂, catalogue no. SC981) was purchased from NeomPS SA (Strasbourg, France). [*myo*-1,2-³H]Inositol with PT6-271 (TRK911, specific activity: 16.0 Ci/mmol) and yttrium silicate (Ysi) RNA binding beads (RPNQ0013) were purchased from GE Healthcare.

Plasmids, Cell Culture, and Membrane Preparation. The cDNAs for guinea pig NK₃ receptor, gpNK₃ (accession number: P30098), was isolated by RT-PCR from a midbrain cDNA library. cDNA encoding the human NK₃ receptor, hNK₃ (accession No. P29371), hNK₂ (accession number: P21452), hNK₁ (accession number: P25103), and gpNK₃ were subcloned into pCI-Neo expression vectors (Promega Corporation, Madison, WI). All point mutants were constructed using the Quick-Change site-directed mutagenesis kit (catalogue no. 200518, Stratagene, La Jolla, CA). The entire coding regions of all point mutants were sequenced from both strands using an automated cycle sequencer (Applied Biosystems, Foster City, CA).

Human embryonic kidney (HEK)293 cells were transfected as previously described.²⁵ Forty-eight hours posttransfection, the cells were harvested and washed three times with ice-cold PBS and frozen at -80 °C. The pellet was suspended in ice-cold 50 mM Tris-HCl pH 7.4 buffer containing 10 mM EDTA (10 × volume) and homogenized with a polytron (Kinematica AG, Basel, Switzerland) for 30 s at 16000 rpm. After centrifugation at 48000g for 30 min at 4 °C, the pellet was suspended again in ice-cold 10 mM Tris pH 7.4 buffer containing 0.1 mM EDTA (10 × volume), homogenized, and spun again as above. The pellet was resuspended in ice-cold 10 mM Tris pH 7.4 buffer containing 0.1 mM EDTA and 10% sucrose (5 × volume). The membrane homogenate was frozen at -80 °C before use.

Radioligand [³H]3** Binding.** After thawing, the membrane homogenates were centrifuged at 48 000g for 10 min at 4 °C, and the pellets were resuspended in the binding buffer (50 mM Tris-HCl, 4 mM MnCl₂, 1 μM phosphoramidon, 0.1% bovine serum albumin at pH 7.4) to a final assay concentration of 5 μg protein/well. Saturation isotherms were determined by addition of various concentrations of radioligand [³H]**3** (0.009 to 3 nM) to these membranes (in a total reaction volume of 500 μL) for 75 min at room temperature (RT). At the end of the incubation, membranes were filtered onto unitfilter (96-well white microplate with bonded GF/C filter preincubated 1 h in 0.3% polyethylenimine + 0.3% bovine serum albumin; PerkinElmer Life and Analytical Sciences, Waltham, MA) with a FilterMate-96 harvester (PerkinElmer Life and Analytical Sciences) and washed 4 times with ice-cold 50 mM Tris-HCl, pH 7.4 buffer.

Nonspecific binding was measured in the presence of 10 μM compound **2**. The radioactivity on the filter was counted (5 min) on a Packard Top-count microplate scintillation counter with quenching correction after addition of 45 μL of microscint 40 (Canberra Packard SA, Zürich, Switzerland) and shaking for 1 h. Saturation experiments were analyzed by Prism 4.0 (GraphPad software, San Diego, CA) using the rectangular hyperbolic equation derived from the equation of a bimolecular reaction and the law of mass action, $B = (B_{\max}[F])/(K_D + [F])$, where B is the amount of ligand bound at equilibrium, B_{\max} is the maximum number of binding sites, $[F]$ is the concentration of free ligand, and K_D is the ligand dissociation constant. For inhibition experiments, membranes were incubated with [³H]**3** at a concentration equal to K_D value of radioligand and 10 concentrations of the inhibitory compound (0.0003–10 μM). IC₅₀ values were derived from the inhibition curve and the affinity constant (K_i) values were calculated using the Cheng-Prussoff equation $K_i = IC_{50}/(1 + [L]/K_D)$ where $[L]$ is the concentration of radioligand and K_D is its dissociation constant at the receptor, derived from the saturation isotherm. The association and dissociation kinetics for radioligand [³H]**3** in the membrane preparations from HEK293 cells transiently expressing hNK₃-WT, gpNK₃-WT, or gpNK₃-A114^{25,58}T were measured as previously described.²⁵ Binding kinetics parameters, K_{ob} and K_{off} values (observed on and off rates), were derived from association–dissociation curves using the one phase exponential association and decay equations (Prism 4.0, GraphPad software), respectively. K_{on} , half-life, and K_d were calculated using the $K_{on} = (K_{ob} - K_{off})/[ligand]$, $t_{1/2} = \ln 2/K$ and $K_d = K_{off}/K_{on}$ equations, respectively.

Radioligands [³H]SP and [³H]4** ([³H]SR 48968) Bindings.** hNK₁ and hNK₂ receptor binding experiments were performed as described above for radioligand [³H]**3** binding, using radioligands [³H]SP and [³H]**4** and membrane isolated from HEK293 transiently expressing recombinant hNK₁ and hNK₂ receptors, respectively. Briefly, after thawing, the membrane homogenates were resuspended and homogenized using a polytron in the 50 mM Hepes, 3 mM MnCl₂, 2 μM phosphoramidon, 16.8 μM Leupeptin, and 0.04% BSA binding buffer at pH 7.4 for the hNK₁ membrane and in the 50 mM Tris-HCl, 3 mM MnCl₂, 4 μg/mL Chymostatin, and 0.04% BSA binding buffer at pH 7.4 for the hNK₂ membrane to a final assay concentration of 2.5 μg protein/well for both NK membranes. For inhibition experiments, hNK₁ and hNK₂ membranes were incubated with 0.6 nM of radioligand [³H]SP ($K_d = 0.6$ nM) and 0.32 nM of radioligand [³H]**4** ($K_d = 0.32$ nM), respectively and 10 concentrations of the inhibitory compound (0.0003–10 μM) (in a total reaction volume of 500 μL) for 75 min at room temperature (RT). Nonspecific bindings for radioligands [³H]SP and [³H]**4** were measured in the presence of 10 μM (2*S*,3*S*)-*cis*-2-(diphenylmethyl)-*N*-[(2-methoxyphenyl)-methyl]-1-azabicyclo[2.2.2]octan-3-amine (CP-96,345)³⁶ and 1-{2-[(*R*)-3-(3,4-dichloro-phenyl)-1-(3,4,5-trimethoxy-benzoyl)-pyrrolidin-3-yl]-ethyl}-4-phenyl-piperidine-4-carboxylic acid amide (MDL 105, 212),³⁷ respectively.

[³H]Inositol Phosphates (IP) Accumulation Assay. [³H]Inositol phosphates accumulation was measured as described previously with the following adaptations.²⁵ The HEK293 cell was transfected with various NK₃ cDNAs in pCI-Neo using Lipofectamine Plus reagent (Invitrogen) according to the manufacturer's instruction. Twenty-four hours after transfection, cells were washed twice in labeling medium: Dulbecco's modified Eagle's medium without inositol (MP Bio-medicals, Irvine, CA), 10% fetal calf serum, 1% penicillin/streptomycin, and 2 mM glutamate. Cells were seeded at 8 × 10⁴ cells/well in poly-D-lysine-treated 96-well plates in the labeling medium supplemented with 5 μCi/mL *myo*-[1,2-³H]-inositol. On the day of assay (48 h post-transfection), cells were washed three times with the buffer (1 × HBSS, 20 mM HEPES, pH 7.4) and then incubated for 10 min at RT in assay buffer (1 × HBSS,

20 mM HEPES, pH 7.4 containing 8 mM LiCl, final concentration, to prevent phosphatidyl-inositide breakdown) prior to the addition of agonists or antagonists. When present, antagonists were incubated for 20 min at 37 °C prior to stimulation with agonist [MePhe⁷]NKB, concentrations ranged from 10 μM to 0.1 nM. After 45 min incubation at 37 °C with [MePhe⁷]NKB, the assay was terminated by the aspiration of the assay buffer and the addition of 100 μL 20 mM formic acid to the cells. After shaking for 30 min at 23 °C, a 40 μL aliquot was mixed with 80 μL of yttrium silicate beads (12.5 mg/mL) that bind to the inositol phosphates (but not inositol) and shaken for 30 min at 23 °C. Assay plates were centrifuged for 2 min at 750g prior to counting on a Packard Top-count microplate scintillation counter with quenching correction (PerkinElmer Life and Analytical Sciences).

Model Building. The hNK₃ 7TMD model, based on the X-ray structure of bovine rhodopsin,³⁸ was previously described.²⁵ In short, the amino acid sequences of hNK₃ and gpNK₃ were aligned to the sequence of bovine rhodopsin using the ClustalW multiple alignment program.²⁵ The alignments were then verified to ensure that conserved residues of the transmembrane regions were aligned and manually adjusted in the second extracellular loop (E2) in order to align the conserved cysteine, which takes part in the disulfide bridges occurring between the third transmembrane segment (TM3) and the second extracellular loop (E2).²⁵ Using this alignment and the X-ray structure of bovine rhodopsin (PDB code: 1u19) as template, the software package MOE (MOE v.2005.05, Chemical Computing Group, Montreal, Quebec, Canada) was used to generate a three-dimensional model of the human NK₃.²⁵ Compound **3** was then manually docked into the binding site according to known structure–activity relationship data and the protein–ligand complex minimized.²⁵ Finally, compound **1** has also been manually docked into the thus obtained hNK₃ model, again according to known structure–activity relationship data.²⁵ These docking modes have been validated in our previous work by site-directed mutagenesis data.²⁵ This original hNK₃ model was subsequently used in the current work to link the observed differences in mode of antagonism with a chemical substructure of compound **3**. Besides, it was used to dock piperidine-based NK₃ antagonists (**5**, **6** and **7**)²⁶ into the binding site. This was achieved by aligning the chemical structures onto the already docked compound **3** and optimizing the conformation of the amide side chain to properly fit into the binding cavity. The Ballesteros–Weinstein numbering scheme of the amino acids in the binding site is given to facilitate the comparison with other GPCRs.³⁹

Acknowledgment. We are grateful to Dr. Josef Schneider for performing NMR spectra. We thank Philippe Jablonski and Walter Vivian for their expert technical assistance.

Supporting Information Available: Preparation, NMR, and MS spectroscopic description of compounds **5**, **6**, and **7**. This material is available free of charge via the Internet at <http://pubs.acs.org>.

References

- Alexander, S. P.; Mathie, A.; Peters, J. A. Guide to Receptors and Channels (GRAC), 3rd edition. *Br. J. Pharmacol.* **2008**, *153*, S1–S209.
- Almeida, T. A.; Rojo, J.; Nieto, P. M.; Pinto, F. M.; Hernandez, M.; Martin, J. D.; Candenas, M. L. Tachykinins and tachykinin receptors: structure and activity relationships. *Curr. Med. Chem.* **2004**, *11*, 2045–2081.
- Severini, C.; Improta, G.; Falconieri-Erspamer, G.; Salvadori, S.; Erspamer, V. The tachykinin peptide family. *Pharmacol. Rev.* **2002**, *54*, 285–322.
- Langlois, X.; Wintmolders, C.; te Riele, P.; Leysen, J. E.; Jurzak, M. Detailed distribution of Neurokinin 3 receptors in the rat, guinea pig and gerbil brain: a comparative autoradiographic study. *Neuropharmacology* **2001**, *40*, 242–253.
- Nagano, M.; Saitow, F.; Haneda, E.; Konishi, S.; Hayashi, M.; Suzuki, H. Distribution and pharmacological characterization of primate NK-1 and NK-3 tachykinin receptors in the central nervous system of the rhesus monkey. *Br. J. Pharmacol.* **2006**, *147*, 316–323.
- Shughrae, P. J.; Lane, M. V.; Merchenthaler, I. In situ hybridization analysis of the distribution of neurokinin-3 mRNA in the rat central nervous system. *J. Comp. Neurol.* **1996**, *372*, 395–414.
- Stoessl, A. J. Localization of striatal and nigral tachykinin receptors in the rat. *Brain Res.* **1994**, *646*, 13–18.
- Tooney, P. A.; Au, G. G.; Chahl, L. A. Tachykinin NK1 and NK3 receptors in the prefrontal cortex of the human brain. *Clin. Exp. Pharmacol. Physiol.* **2000**, *27*, 947–949.
- Albert, J. S. Neurokinin antagonists and their potential role in treating depression and other stress disorders. *Expert Opin. Ther. Pat.* **2004**, *14*, 1421–1433.
- Lecci, A.; Maggi, C. A. Peripheral tachykinin receptors as potential therapeutic targets in visceral diseases. *Expert Opin. Ther. Targets* **2003**, *7*, 343–362.
- Quartara, L.; Altamura, M. Tachykinin receptors antagonists: from research to clinic. *Curr. Drug Targets* **2006**, *7*, 975–992.
- Dawson, L. A.; Cato, K. J.; Scott, C.; Watson, J. M.; Wood, M. D.; Foxtan, R.; de la Flor, R.; Jones, G. A.; Kew, J. N.; Cluderay, J. E.; Southam, E.; Murkitt, G. S.; Gartlon, J.; Pemberton, D. J.; Jones, D. N.; Davies, C. H.; Hagan, J. In vitro and in vivo characterization of the non-peptide NK3 receptor antagonist SB-223412 (talnetant): potential therapeutic utility in the treatment of schizophrenia. *Neuropsychopharmacology* **2008**, *33*, 1642–1652.
- Marco, N.; Thirion, A.; Mons, G.; Bougault, I.; Le Fur, G.; Soubrie, P.; Steinberg, R. Activation of dopaminergic and cholinergic neurotransmission by tachykinin NK3 receptor stimulation: an in vivo microdialysis approach in guinea pig. *Neuropeptides* **1998**, *32*, 481–488.
- Emonds-Alt, X.; Bichon, D.; Ducoux, J. P.; Heaulme, M.; Miloux, B.; Poncelet, M.; Proietto, V.; Van Broeck, D.; Vilain, P.; Neliat, G.; et al. SR 142801, the first potent non-peptide antagonist of the tachykinin NK3 receptor. *Life Sci.* **1995**, *56*, PL27–PL32.
- Nguyen-Le, X. K.; Nguyen, Q. T.; Gobeil, F.; Pheng, L. H.; Emonds-Alt, X.; Brelriere, J. C.; Regoli, D. Pharmacological characterization of SR 142801: a new non-peptide antagonist of the neurokinin NK-3 receptor. *Pharmacology* **1996**, *52*, 283–291.
- Giardina, G. A.; Raveglia, L. F.; Grugni, M.; Sarau, H. M.; Farina, C.; Medhurst, A. D.; Graziani, D.; Schmidt, D. B.; Rigolio, R.; Luttmann, M.; Cavagnera, S.; Foley, J. J.; Vecchietti, V.; Hay, D. W. Discovery of a novel class of selective non-peptide antagonists for the human neurokinin-3 receptor. 2. Identification of (S)-N-(1-phenylpropyl)-3-hydroxy-2-phenylquinoline-4-carboxamide (SB 223412). *J. Med. Chem.* **1999**, *42*, 1053–1065.
- Sarau, H. M.; Griswold, D. E.; Potts, W.; Foley, J. J.; Schmidt, D. B.; Webb, E. F.; Martin, L. D.; Brawner, M. E.; Elshourbagy, N. A.; Medhurst, A. D.; Giardina, G. A.; Hay, D. W. Nonpeptide tachykinin receptor antagonists: I. Pharmacological and pharmacokinetic characterization of SB 223412, a novel, potent and selective neurokinin-3 receptor antagonist. *J. Pharmacol. Exp. Ther.* **1997**, *281*, 1303–1311.
- Spooren, W.; Riemer, C.; Meltzer, H. Opinion: NK3 receptor antagonists: the next generation of antipsychotics? *Nat. Rev. Drug Discovery* **2005**, *4*, 967–975.
- Meltzer, H. Y.; Arvanitis, L.; Bauer, D.; Rein, W. Placebo-controlled evaluation of four novel compounds for the treatment of schizophrenia and schizoaffective disorder. *Am. J. Psychiatry* **2004**, *161*, 975–984.
- Liem-Moolenaar, M.; Gray, F.; de Visser, S.; Franson, K.; Schoemaker, R.; Schmitt, J.; Cohen, A.; van Gerven, J. Psychomotor and cognitive effects of a single oral dose of talnetant (SB223412) in healthy volunteers compared with placebo or haloperidol. *J. Psychopharmacol.* **2008**, *21*, 21.
- Oury-Donat, F.; Carayon, P.; Thurneyssen, O.; Pailhon, V.; Emonds-Alt, X.; Soubrie, P.; Le Fur, G. Functional characterization of the nonpeptide neurokinin3 (NK3) receptor antagonist, SR142801 on the human NK3 receptor expressed in Chinese hamster ovary cells. *J. Pharmacol. Exp. Ther.* **1995**, *274*, 148–154.
- Beaujouan, J. C.; Saffroy, M.; Torrens, Y.; Glowinski, J. Potency and selectivity of the tachykinin NK3 receptor antagonist SR 142801. *Eur. J. Pharmacol.* **1997**, *319*, 307–316.
- Patacchini, R.; Bartho, L.; Holzer, P.; Maggi, C. A. Activity of SR 142801 at peripheral tachykinin receptors. *Eur. J. Pharmacol.* **1995**, *278*, 17–25.
- Tian, G.; Wilkins, D.; Scott, C. W. Neurokinin-3 receptor-specific antagonists talnetant and osanetant show distinct mode of action in cellular Ca²⁺ mobilization but display similar binding kinetics

- and identical mechanism of binding in ligand cross-competition. *Mol. Pharmacol.* **2007**, *71*, 902–911.
- (25) Malherbe, P.; Bissantz, C.; Marcuz, A.; Kratzeisen, C.; Zenner, M. T.; Wettstein, J. G.; Ratni, H.; Riemer, C.; Spooren, W. Metalnetant and osanetant interact within overlapping but not identical binding pockets in the human tachykinin neurokinin 3 receptor transmembrane domains. *Mol. Pharmacol.* **2008**, *73*, 1736–1750.
- (26) Knust, H.; Nettekoven, M. H.; Ratni, H.; Vifian, W.; Wu, X. Piperidine derivatives as NK3 receptor antagonists. WO 2009/033995 A1, **2009**.
- (27) Meltzer, H.; Prus, A. NK3 receptor antagonists for the treatment of schizophrenia. *Drug Discovery Today: Ther. Strategies* **2006**, *3*, 555–560.
- (28) Chung, F. Z.; Wu, L. H.; Tian, Y.; Vartanian, M. A.; Lee, H.; Bikker, J.; Humblet, C.; Pritchard, M. C.; Raphy, J.; Suman-Chauhan, N.; et al. Two classes of structurally different antagonists display similar species preference for the human tachykinin neurokinin3 receptor. *Mol. Pharmacol.* **1995**, *48*, 711–716.
- (29) Wu, L. H.; Vartanian, M. A.; Oxender, D. L.; Chung, F. Z. Identification of methionine134 and alanine146 in the second transmembrane segment of the human tachykinin NK3 receptor as reduces involved in species-selective binding to SR 48968. *Biochem. Biophys. Res. Commun.* **1994**, *198*, 961–966.
- (30) Leffler, A.; Ahlstedt, I.; Engberg, S.; Svensson, A.; Billger, M.; Oberg, L.; Bjursell, M. K.; Lindstrom, E.; von Mentzer, B. Characterization of species-related differences in the pharmacology of tachykinin NK receptors 1, 2 and 3. *Biochem. Pharmacol.* **2009**, *77*, 1522–1530.
- (31) Cassel, J. A.; Daubert, J. D.; DeHaven, R. N. [(3)H]Alvimopan binding to the micro opioid receptor: comparative binding kinetics of opioid antagonists. *Eur. J. Pharmacol.* **2005**, *520*, 29–36.
- (32) Copeland, R. A.; Pompliano, D. L.; Meek, T. D. Drug-target residence time and its implications for lead optimization. *Nat. Rev. Drug Discovery* **2006**, *5*, 730–739.
- (33) Lacourciere, Y.; Asmar, R. A comparison of the efficacy and duration of action of candesartan cilexetil and losartan as assessed by clinic and ambulatory blood pressure after a missed dose, in truly hypertensive patients: a placebo-controlled, forced titration study. Candesartan/Losartan study investigators. *Am. J. Hypertens.* **1999**, *12*, 1181–1187.
- (34) Swinney, D. C. Biochemical mechanisms of drug action: what does it take for success? *Nat. Rev. Drug Discovery* **2004**, *3*, 801–808.
- (35) Swinney, D. C. The role of binding kinetics in therapeutically useful drug action. *Curr. Opin. Drug Discovery Dev.* **2009**, *12*, 31–39.
- (36) Lowe, J. A., III; Drozda, S. E.; Snider, R. M.; Longo, K. P.; Zorn, S. H.; Morrone, J.; Jackson, E. R.; McLean, S.; Bryce, D. K.; Bordner, J.; et al. The discovery of (2*S*,3*S*)-*cis*-2-(diphenylmethyl)-*N*-[(2-methoxyphenyl)methyl]-1-azabicyclo[2.2.2]octan-3-amine as a novel, nonpeptide substance P antagonist. *J. Med. Chem.* **1992**, *35*, 2591–2600.
- (37) Burkholder, T. P.; Kudlacz, E. M.; Le, T.-B.; Knippenberg, R. W.; Shatzer, S. A.; Maynard, G. D.; Webster, M. E.; Horgan, S. W. Identification and chemical synthesis of MDL 105,212, a non-peptide tachykinin antagonist with high affinity for NK1 and NK2 receptors. *Bioorg. Med. Chem. Lett.* **1996**, *6*, 951–956.
- (38) Palczewski, K.; Kumasaka, T.; Hori, T.; Behnke, C. A.; Motoshima, H.; Fox, B. A.; Le Trong, I.; Teller, D. C.; Okada, T.; Stenkamp, R. E.; Yamamoto, M.; Miyano, M. Crystal structure of rhodopsin: A G protein-coupled receptor. *Science*. **2000**, *289*, 739–745.
- (39) Ballesteros, J. A.; Weinstein, H. Integrated methods for construction three-dimensional models and computational probing of structure-function relations in G protein-coupled receptors. *Methods Neurosci.* **1995**, *25*, 366–428.